An Adaptive Power Oscillation Damping Controller for a Hybrid AC/DC Microgrid

MOUDUD AHMED[ID]**, (Student Member, IEEE), ARASH VAHIDNIA, (Senior Member, IEEE),**
MANOJ DATTA[ID]**, (Senior Member, IEEE), AND**
LASANTHA MEEGAHAPOLA[ID]**, (Senior Member, IEEE)**
School of Engineering, RMIT University, Melbourne, VIC 3000, Australia

Corresponding author: Moudud Ahmed (s3636503@student.rmit.edu.au)

ABSTRACT High penetration of dynamic loads, such as induction motors (IMs) could give rise to sustained voltage/frequency and power oscillations in hybrid AC/DC microgrids during disturbances. Majority of the published literature has investigated these stability issues with aggregated models of IMs in hybrid AC/DC microgrids, which do not properly reflect the actual dynamics of parallel operating IMs; hence, power oscillation damping (POD) controllers must be designed explicitly considering various oscillations induced by parallel operating IMs. This paper proposes an adaptive neuro-fuzzy inference system (ANFIS) based POD controller to damp low-frequency oscillations (LFOs) induced by IMs in hybrid AC/DC microgrids. The proposed supplementary POD controller was embedded to the energy storage system (ESS) controller, which provides additional damping power proportional to the frequency deviation. The following two features namely: 1) ability to adjust the gain based on the frequency deviation, and 2) ability to handle more non-linearity in the system dynamics, make the proposed adaptive ANFIS based POD controller more unique compared to conventional POD controllers. The effectiveness of the proposed ANFIS-POD controller is verified using non-linear dynamic simulations considering a range of disturbances in a hybrid AC/DC microgrid and different combinations of parallel operating IMs. Results indicate improved oscillatory stability performance in the hybrid AC/DC microgrid with the proposed ANFIS-POD controller.

NOMENCLATURE

AC:	Alternating current
ANN:	Artificial neural network
ANFIS:	Adaptive neuro-fuzzy inference system
CPL:	Constant power load
DC:	Direct current
DGIG:	Doubly-fed induction generator
ESS:	Energy storage system
FIS:	Fuzzy inference system
ILC:	Interlinking converter
IM:	Induction motor
LFO:	Low-frequency oscillation
MPPT:	Maximum power point tracking
NA:	Non adaptive
NC:	No controller
PCC:	Point of common coupling
PEC:	Power electronic converter
PSS:	Power system stabilizer
POD:	Power oscillation damping
PSD:	Power spectrum density
RES:	Renewable energy source
SOC:	State of charge
VSC:	Voltage source converter

I. INTRODUCTION

Advancement of power electronic converter (PEC) interfaced renewable energy sources (RESs), and energy storage systems (ESSs) have paved the way to a new energy system architecture called "microgrids". The PEC-interfaced RESs have a high degree of controllability & operability compared to the synchronous generator which can enhance the reliability, stability, economics, and sustainability of the power system [1]. Concurrently, the large-scale integration of PEC-interfaced RESs have changed the unidirectional power-flow from the conventional generating stations to loads

through transmission & distribution networks to a bidirectional power flow by necessitating more complex coordinated control schemes for both power grids and microgrids. Both the direct current (DC) and the alternating current (AC) based renewable resources and loads are being connected to microgrids. This has paved the way to the hybrid AC/DC microgrid concept, which has gained enormous popularity in recent years as it combines the advantages of both the AC and the DC microgrids [2], [3]. The hybrid AC/DC microgrid can be operated either in autonomous mode (i.e., disconnected from the distribution network) or grid-connected mode (i.e., connected to the utility grid). The control of RESs in autonomous mode is a critical issue for the advancement of hybrid AC/DC microgrids. One well-established droop control method is employed to mimic the behaviour of synchronous generators and hence ensure autonomous operation [4].

The hybrid AC/DC microgrid may become unstable during the autonomous operation mode due to abnormal weather conditions, faults and load dynamics [5]. Small-signal stability of droop controlled autonomous AC microgrids have been studied in [6]–[8], and these studies have identified frequency oscillations as a major stability issue in microgrids. The LCL filter parameters, inner current and outer voltage controllers affect the medium and the high-frequency oscillation modes, whereas droop controller parameters and load demand affect the low-frequency oscillation (LFO) modes. To study the stability of a hybrid AC/DC microgrid with the induction motor (IM) load, a small-signal stability analysis has been conducted in [9]. According to the study, IMs significantly influence the dynamic performance & stability of the entire hybrid AC/DC microgrid and have introduced LFO modes. Moreover, the droop gain of the VSC is small with IM load compared to the static load. It means that small droop gain improves the stability limit of the hybrid AC/DC microgrid with dynamic loads, however will result in poor power-sharing performance. Furthermore, research studies conducted to evaluate the influence of the microgrid cable/feeder characteristics (e.g. X/R ratio) on hybrid AC/DC microgrid dynamic stability have revealed that the cable/ feeder characteristics have some influence on LFOs emanating from IMs [10], [11].

In the power system, a significant share of power is consumed by the IM in industrial, agricultural, and commercial applications, which constitute 60% to 70% of total energy [12]. Moreover, the IM is considered as a dynamic load, because their dynamics change with the change of the system operating conditions (i.e., voltage & frequency). Due to the increased use of IMs in residential, commercial and industrial applications, hybrid AC/DC microgrids are subjected to a wide range of IM loading configurations. Previous research studies [13], [14] have reported that the IM significantly influence the damping of oscillations in power systems and a large number of IMs with different ratings are aggregated for damping analysis. The impact of multiple IM loads on dynamic performance and microgrid stability has

investigated in [15], which shows that single large IM has single dominant oscillation frequency, while multiple parallel operating small IMs have multiple dominant oscillation frequencies. It means that multiple parallel operating IMs have introduced more non-linearity into hybrid AC/DC microgrid dynamics.

In authors' previous work [16], a supplementary power oscillation damping (POD) controller is implemented in the ESS controller to damp out the oscillations. The supplementary POD controller adds an additional signal to the ESS controller proportional to the frequency deviation. This supplementary POD controller can significantly damp LFOs in the hybrid AC/DC microgrid. However, the following two attributes, 1) if the gain of the proportional based POD controllers can be adjusted with the IM loading level, 2) if the proportional controller is effective over a wide-range of operating conditions, can make the LFO damping performance even better under various combinations of IMs in microgrids. The frequency deviation is increased with the increase of dynamic load, which requires more damping torque. However, the proportional based POD controller is incapable of changing its gain based on the frequency deviation. To incorporate the aforementioned features, this research study proposed an adaptive neuro-fuzzy inference system (ANFIS) based POD controller for the ESS controller, which can handle highly non-linear system dynamics [17]–[19]. Although the conventional POD controllers could damp out LFOs, the ANFIS based adaptive POD controller is even better, since they can mitigate oscillations more effectively under varying dynamic loads, such as IMs.

ANFIS is a fuzzy inference system (FIS) implemented in an adaptive network framework. An ANFIS has the inherent capability of learning and parallel data processing which combines the advantages of both the artificial neural network (ANN) and the fuzzy logic. The uncertainty handling capability of the ANFIS has been proved to be advantageous, since the hybrid AC/DC microgrid is operating with non-linear dynamic loads [20]–[22]. The proposed ANFIS based POD controller adapts to the non-linear states of the AC sub-grid system frequency and adjusts the gain of the POD controller to damp out the oscillations. This paper proposes an ANFIS based POD controller for the ESS controller of a hybrid AC/DC microgrid, where ESS is connected to the AC sub-grid. The power transfer between the AC & the DC sub-grids is regulated by the interlinking converter (ILC). This research makes the following contributions;

- This research identifies the IM rotor speed oscillations and compares the damping performance of the non-adaptive POD controller with different IM loading levels, while the controller parameters remain unchanged.
- This research also investigates the LFO characteristics for different combinations of multiple parallel operating IMs of same power ratings.

- This research proposes an ANFIS based POD controller, which autonomously adjusts its gain based on IM loading level and provides significantly improved response over a wide-range of operating conditions.
- The robustness of the proposed controller is verified by applying various disturbances at both sides of the hybrid AC/DC microgrid with various combinations of parallel operating IMs of distinct power ratings, while total IM loading level remains unchanged.

The rest of the paper is structured as follows: Section II describes the dynamic simulation platform. The necessity for an adaptive POD controller is discussed in Section III. Section IV describes the detailed design procedure of the ANFIS-POD and the ESS controllers. Simulation results with case studies are presented in Section V, and finally, the conclusions of this research study are presented in Section VI.

II. DESCRIPTION OF THE SIMULATION PLATFORM

The hybrid AC/DC microgrid model illustrated in Fig. 1 was based on the model given in [16]. The control parameters of the individual DERs are taken from [16]. As it is a low voltage weak distribution microgrid, the reactance to resistance (X/R) ratio of each cable connecting each DER to the PCC of the AC sub-grid is 0.4. The AC sub-grid voltage and frequency are maintained at 400 V and 50 Hz, whereas the DC sub-grid voltage is maintained at 650 V.

Parallel connection of solar-PV systems could improve the overall reliability of the solar-PV generation [23], and hence two parallel solar-PV systems, each rated at 250 kW generation capacity (interfaced to a 300 kVA VSC) are connected to the AC sub-grid. The 250 kW solar-PV system consists of 88 parallel strings with 7 modules per each string. The voltage and the current at the maximum power point (MPP) for each module are 72.9 V and 5.69 A respectively. A 400 kW doubly-fed induction generator (DFIG) is connected to the AC sub-grid via a back to back power electronic converter. The input wind speed at the DFIG wind turbine is fixed at rated speed (i.e., 12 m/s). A 500 kVA lithium-ion battery bank is connected to the AC sub-grid of the hybrid AC/DC microgrid. The battery bank state-of-charge (SOC) is maintained at 90%. The ampere-hour capacity of the battery bank is 850 Ah (552.5 kWh), and open-circuit voltage is 650 V respectively.

According to the investigation carried out in the Ontario hydro system found that the total IM load configuration consists of 28.90% small residential IMs, 18.1376% medium commercial IMs, and 52% large industrial IMs [24]. Therefore, the IM loading configuration of the test system consists of IMs with different power ratings, which mimic the practical IM loading configurations as listed in Table 1.

The AC sub-grid and the DC sub-grid are connected via a 500 kVA ILC. The ILC controller was developed to facilitate the power transfer between AC and DC sub-grids and to assist
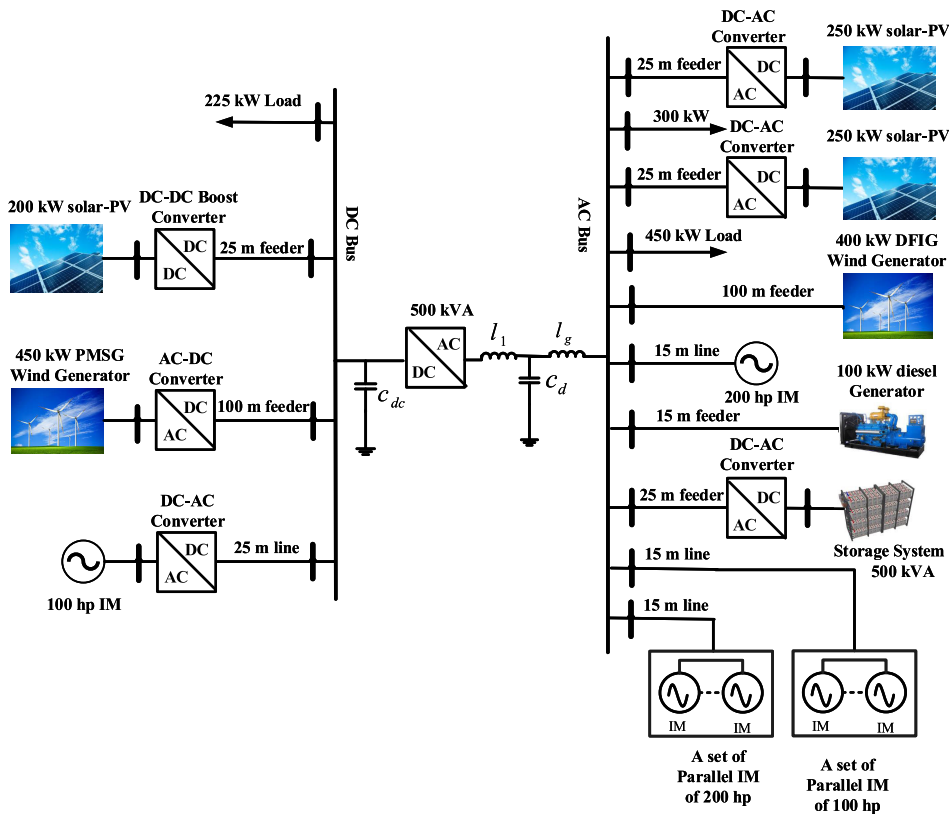

FIGURE 1. The hybrid AC/DC microgrid model.

TABLE 1. Different IM loading configurations.

Combination of IM's	Mode
1×200 hp IM, 40×5 hp IM, and 4×25 hp IM	Mode-1
1×200 hp IM, 20×10 hp IM, and 2×50 hp IM	Mode-2
1×200 hp IM, 10×20 hp IM, and 7×15 hp IM	Mode-3

the AC sub-grid to operate in the autonomous mode. The ILC controller has outer voltage and inner current control loops where the outer voltage control loop determines the power dispatch from AC to DC or DC to AC sub-grids. The DC link filter capacitor (C_{dc}) and LCL filter at the ILC are used to maintain a stable voltage at both the AC and the DC sub-grids. The total generation capacity of the DC sub-grid is 650 kW. A 200 kW solar-PV system with a DC-DC boost converter, and a 450 kW permanent magnet synchronous generator (PMSG) is connected to the DC sub-grid. The 200 kW solar PV-array consists of 72 parallel strings with 7 modules per each string. A DC load of 225 kW as a constant impedance load and an IM of 100 hp IM through a DC-AC converter as a constant power load (CPL) are connected to the DC sub-grid, respectively. In contrast to the constant impedance loads, CPLs will draw constant amount of power regardless of the DC sub-grid voltage.

III. REQUIREMENTS FOR AN ADAPTIVE POD CONTROLLER

For the 300 kW step load addition scenario, the rotor speed with no controller (NC) and non-adaptive (NA) controller (based on [16]) is illustrated in Fig. 2(a), where a single 200-hp IM is used as a dynamic load. The voltage and frequency oscillations in the AC sub-grid are caused by the load disturbances, which subsequently caused IM

rotor speed oscillations. It can be seen from Fig. 2 (a) that IM's rotor have significant oscillations, and improvement is achieved by implementing a NA-POD controller. Later on the dynamic load is increased by adding another 200-hp IM to the AC sub-grid and the rotor speed oscillations were observed while the setting of the NA-POD controller remained unchanged. The IM rotor speed oscillations with single 200-hp IM and two 200-hp IM are illustrated in Fig. 2 (b), which shows insufficient damping performance of the NA-POD controller for the two 200-hp IM loading conditions. Basically, the NA-POD controller provides a supplementary control signal to the ESS controller proportional to speed/frequency deviation. The gain of the NA-POD controller is fixed and can not be changed with the loading condition of the system. Therefore, under high IM loading level more speed/frequency deviations can be expected, and hence more damping (D) torque is required to damp speed oscillations as D is proportional to the speed/frequency (ω) deviation ($D \propto \omega$) [25].

Now, the microgrid IM loading configuration is changed to mode-1 (i.e., one 200 hp IM, forty 5 hp IM, and four 25 hp IM) and the performance of the NA-POD is evaluated by applying the aforementioned load disturbances which is depicted in Fig. 2(c). With the same setting of the POD controller, it provides little improvement in damping performance compared with NC. The power spectrum density (PSD) analysis of the AC sub-grid system frequency with 40 parallel 5-hp IMs and single 200-hp IM is illustrated in Fig. 3(a). It can be inferred that the system frequency (Fig. 3(a)) has one dominant oscillation frequency around
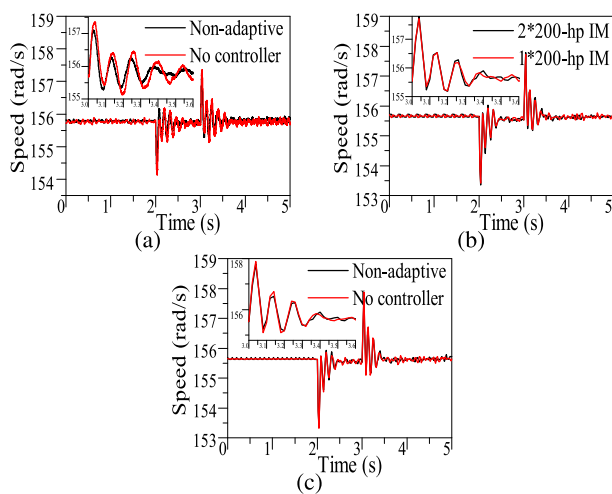

FIGURE 2. IM rotor speed characteristics; (a) Rotor speed, (b) Rotor speed with one & two 200-hp IM, (c) Rotor speed with mode-1 IM loading configuration.
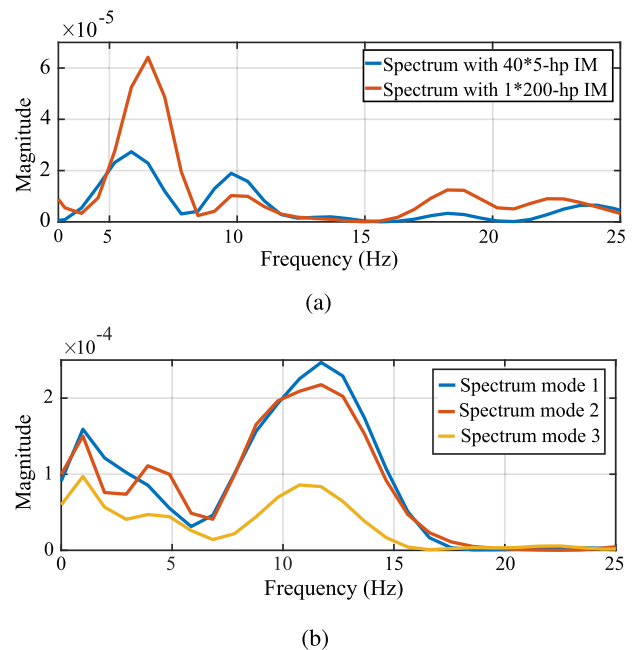

FIGURE 3. Power spectral density of the system frequency; (a) Spectrum of forty 5-hp IM and 1-200-hp IM, (b) Spectrum of three different mode IM loading configuration.

5 Hz in the case of single 200-hp IM, whereas the system frequency with 40 parallel 5-hp IMs has multiple dominant oscillation frequencies of around 5 Hz and 10 Hz. Similarly, the power spectrum of the AC sub-grid frequency with three distinct IM modes (shown in Table 1) is presented in Fig. 3(b). It can be seen from Fig. 3(b) that each IM loading mode has three dominant frequencies which shows the increased non-linearity of the hybrid AC/DC microgrid. To achieve better damping performance from the POD controller, the following control requirements should be satisfied:

- Autonomous adjustment of the gain of the POD controller with the different IM loading configurations.
- Provide better response over a wide range of operating conditions, i.e., tackle the non-linearity of the system dynamics.

A. NON-ADAPTIVE CONTROLLER WITH COMPENSATOR FOR SPECIFIC OSCILLATION FREQUENCY

The traditional power system stabilizer (PSS) used in the synchronous generator excitation system is utilized as the POD controller to damp inter-area electro-mechanical oscillations [25]. The POD controller provides a supplementary in-phase damping torque component with speed/frequency deviation where the lead/lag compensation block maintains the appropriate phase. The lead/lag compensation block parameters are designed based on the frequency of oscillation that must be damped. A series of lead/lag compensation block is utilized in the POD controller to damp different oscillatory modes such as inter-area, local, and global oscillation modes [26]–[28]. A lead/lag compensator is added after the washout filter (Fig. 6(a)) with the NA-POD controller. The lead/lag compensation block is designed for 5.0 Hz ($s = j\omega = 5.0s$) i.e., 5.0 Hz LFO has to be damped. For the 300 kW step load addition scenario, the rotor speed with a non-adaptive POD controller (based on (2)) and non-adaptive POD controller with lead/lag compensator is illustrated in Fig. 4 (a), where two 200-hp IM is used as a dynamic load. The lead/lag compensator adds a zero and damp rotor speed oscillation compared to the POD controller without the compensator.

Now, IM rotor speed with a non-adaptive POD controller with lead/lag compensator is illustrated in Fig. 4 (b); where two distinct loading level are used, 1) two 200-hp IM, 2) single 200-hp IM and 40 parallel 5-hp IMs. It can be seen from (Fig. 4 (b)) that the non-adaptive POD controller with lead/lag compensator damping performance deteriorates when the load characteristics are changed. It can be inferred from the system frequency PSD analysis (Fig. 3(a)) that 40 parallel operating 5-hp IM introduces two oscillating frequencies around 5 Hz and 10 Hz respectively. However, the POD controller lead/lag compensator was designed for 5.0 Hz oscillating frequency which results poor damping performance. Therefore, the POD controller with series lead/lag compensator is capable of damping oscillation if the frequency of oscillation is known and the compensator is designed based
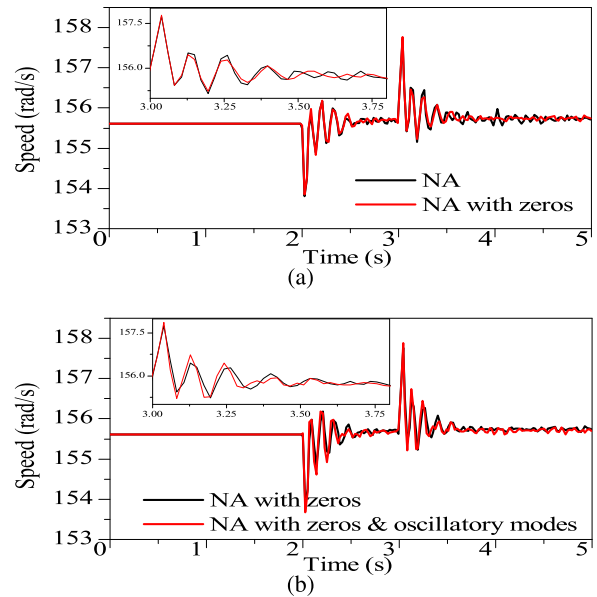
FIGURE 4. IM rotor speed characteristics; (a) Non-adaptive controller with and without zeros, (b) Non-adaptive with zeros and zeros & oscillatory modes.

on that particular oscillation frequency. However, in this research, the nature of oscillation frequency is unknown, and it is originating from the IM loads (dynamic loads).

IV. ENERGY STORAGE SYSTEM WITH ADAPTIVE POD CONTROLLER

The detailed control diagram of the ESS controller is illustrated in Fig. 5, it comprises outer voltage control loop with a supplementary ANFIS based POD controller, outer frequency control loop, and inner current control loop. The amount of power injected by the ESS is determined by the outer voltage/frequency control loop and inner current control loop. The detailed description of the control parameter selection procedure of the outer voltage/frequency controller and inner current controller can be found in the authors previous work [16]. The non-adaptive and the ANFIS based adaptive POD controllers are illustrated in Fig. 6 (a) and (b) respectively. The design process of these POD controllers are discussed in the subsequent section.

A. NON-ADAPTIVE POD CONTROLLER

The non-adaptive POD controller comprises a proportional controller, a low-pass filter, and a wash-out filter block. The transfer function of the POD controller is given by;

$$H(s) = k_D \cdot \left(\frac{1}{(1 + sT_L)} \right) \cdot \left(\frac{sT_F}{(1 + sT_F)} \right) \tag{1}$$

where, T_L, T_F, and k_D, are low-pass filter time constant, the wash-out filter time constant, and proportional controller gain respectively. The scalar gain of the proportional controller is fixed at 150, while the wash-out filter and the low-pass filter time constants are chosen as 10 s and 0.2 s respectively to
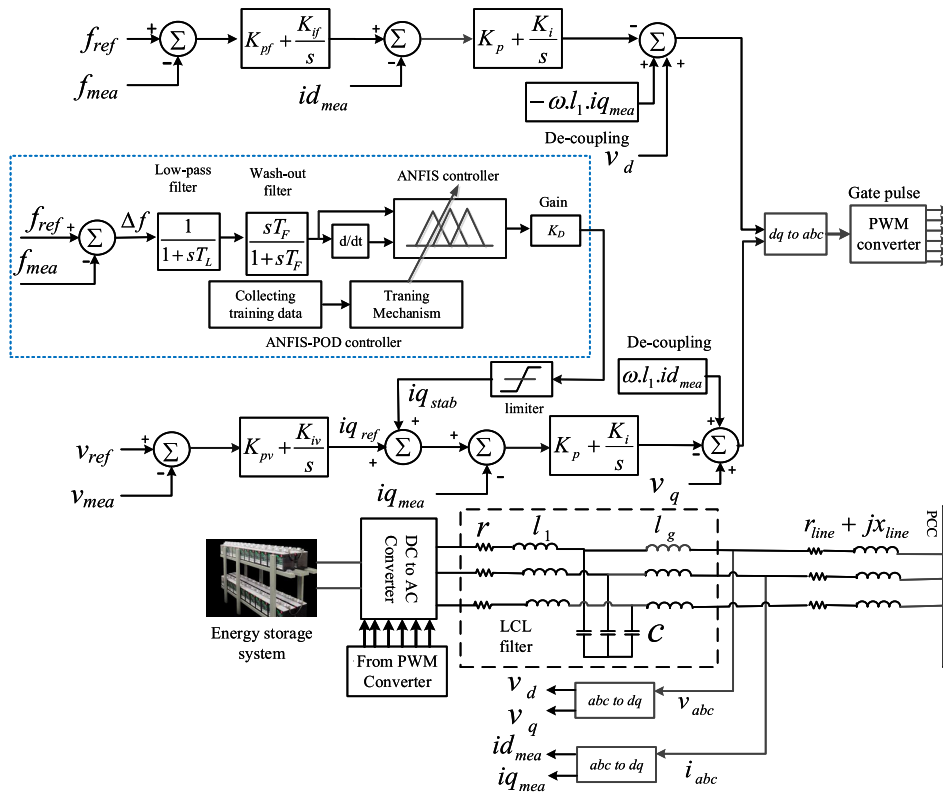
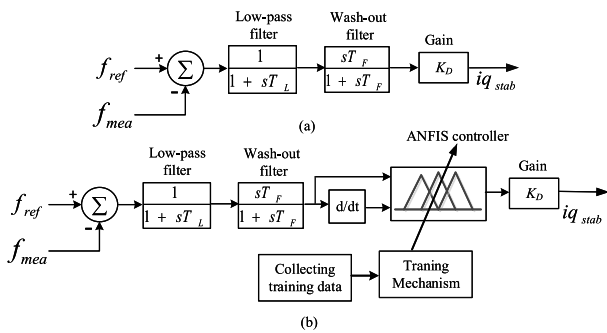**FIGURE 5.** The ESS controller with an adaptive POD controller.

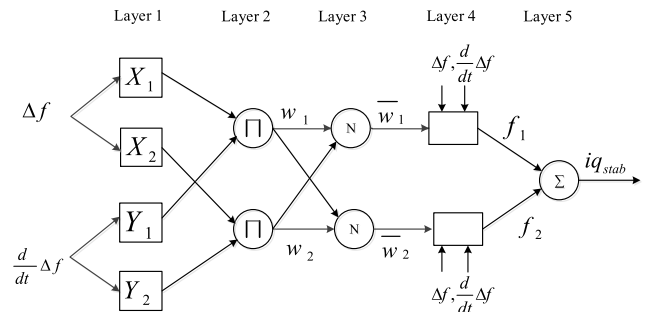**FIGURE 6.** POD controller, (a) Non-adaptive, (b) Adaptive.

FIGURE 7. ANFIS control architecture [19].

pass the LFO unaltered to the POD controller. Therefore, the transfer function of the non-adaptive POD controller takes the following form;

$$H(s) = \frac{1500s}{2s^2 + 10.2s + 1} \qquad (2)$$

B. ANFIS BASED ADAPTIVE POD CONTROLLER

An ANFIS based adaptive control scheme has been designed as the supplementary controller of the outer voltage control loop of the ESS controller. This supplementary POD controller provides additional control signal proportional to the AC sub-grid frequency deviation. An ANFIS is a combination

of ANN and fuzzy logic, which has learning and parallel data processing capabilities [19], [29]. The general architecture of the ANFIS is depicted in Fig. 7, which consists of five layers, i.e., an input layer, three hidden layers, and an output layer; and each layer or node are connected through directional links. Three basic steps should be followed to design ANFIS; (1) learning paradigm, which means learning process based on the system information; (2) learning algorithm, which refers to a rule that is used to adjust the synapses and parameters of the ANFIS; and (3) assess the network capacity and samples required for training to train the network [30]. The deviation of the frequency (Δf) from the reference point and the prediction of future deviation, i.e. derivation of frequency

deviation ($\frac{d}{dt}\Delta f$) from the reference set point are given as input to the ANFIS based adaptive POD controller. The basic rules used in the Takagi-Sugeno type ANFIS is given bellow;

$$if\,(\Delta f = X_1)\&(\frac{d}{dt}\Delta f = Y_1),\;then\,f_1 = p_1\Delta f + q_1\frac{d}{dt}\Delta f + r_1$$
$$if\,(\Delta f = X_2)\&(\frac{d}{dt}\Delta f = Y_2),\;then\,f_2 = p_2\Delta f + q_2\frac{d}{dt}\Delta f + r_2$$
$$(3)$$

where, X_1, X_2 and Y_1, Y_2 are fuzzy sets, while p_1, p_2, q_1, q_2, r_1, and r_2 are the consequent parameters.

Layer 1: The input variables are applied to the layer 1 to obtain the fuzzy sets corresponding to the input variables. Every node in layer 1 is a square node which gives the membership value of each input variables as follows;

$$O_i = \mu X_i(\Delta f)$$
$$O_i = \mu Y_i(\frac{d}{dt}\Delta f) \qquad (4)$$

Here, i is the node number, X_i(or Y_i) is a linguistic level, and O_i is the membership function (MF) of X_i or Y_i. In this research, Gaussian MF is chosen (μX_i) and is defined as follows;

$$\mu X_i(\Delta f) = e^{\frac{-1}{2}(\frac{x-c}{\sigma})^2}$$
$$\mu Y_i(\frac{d}{dt}\Delta f) = e^{\frac{-1}{2}(\frac{x-c}{\sigma})^2} \qquad (5)$$

where σ, c determines the width and the center of the membership function respectively. These parameters of the membership function are known as premise parameters.

Layer 2: Layer 2 nodes are circle nodes and they multiply the incoming signals coming from layer 1. The output of the layer 2 is given as follows;

$$O_{2,i} = W_i = \mu X_i(\Delta f) \times \mu Y_i(\frac{d}{dt}\Delta f) \qquad (6)$$

Here, firing strength of each node is denoted by W_i.

Layer 3: Layer 3 nodes are circle nodes and the number of fuzzy rules are equal to the number of layers. The output of the ith node is the ratio of ith node firing strength to the weighted sum of all nodes firing strengths, as formulated bellow;

$$O_{3,i} = \bar{W}_i = \frac{W_i}{\Sigma(W_1 + W_2)} \qquad (7)$$

Layer 4: Layer 4 nodes are circle nodes and output node function can be formulated as follows;

$$O_{4,i} = f_1 = \bar{W}_1(p_1\Delta f + q_1\frac{d}{dt}\Delta f + r_1)$$
$$O_{4,i} = f_2 = \bar{W}_2(p_2\Delta f + q_2\frac{d}{dt}\Delta f + r_2) \qquad (8)$$

Layer 5: Layer 5 provides the ANFIS final output by summing all the incoming signals from previous layer. The output signal (iq_{stab}) can be formulated as follows;

$$O_{5,i} = iq_{stab} = \Sigma(f_1 + f_2) \qquad (9)$$

The ANFIS controller has to set the values of the premise and the consequent parameters by the forward pass and the backward pass respectively. In the forward pass, consequent parameters are evaluated, while premise parameters kept constant, whereas in the backward pass, premise parameters are evaluated while consequent parameters are kept constant. Now, consider that the training data set has N number of input data, the error function for the nth ($1 \leq n \leq N$) training data set can be formulated as follows;

$$E_n = \sum_{p=1}^{m}(T_{p,n} - O_{p,n}^m)^2 \qquad (10)$$

where, $O_{p,n}$, $T_{p,n}$, and E_n are the pth component of the nth output vector, reference output vector, and error respectively. Therefore, the total measured error is:

$$E = \sum_{n=1}^{N} E_n \qquad (11)$$

The rate of error at node (m, i) from (10) can be formulated as;

$$\frac{\delta E_n}{\delta O_{i,n}^m} = -2(T_{i,n} - O_{i,n}^m) \qquad (12)$$

If σ is a parameter of the ANFIS, then rate of change of error with respect to σ is;

$$\frac{\delta E_n}{\delta \sigma} = \sum_{O\varepsilon S} \frac{\delta E_n}{\delta O}\frac{\delta O}{\delta \sigma}$$
$$\frac{\delta E}{\delta \sigma} = \sum_{n=1}^{N}\frac{\delta E_n}{\delta \sigma} \qquad (13)$$

Here, S denotes the nodes whose output depends on σ. Also, $\frac{\delta E}{\delta \sigma}$ denotes the rate of change of the total measured error with respect to σ. Therefore, updated generic parameter, σ can be written as;

$$\Delta\sigma = -\beta\frac{\delta E}{\delta \sigma}$$
$$\beta = -\frac{J}{\sqrt{\sum_\sigma(\frac{\delta E}{\delta \sigma})^2}} \qquad (14)$$

where β is the learning rate and J is the step size, which is varied to enhance the rate of convergence. Off-line learning is used to update σ based on (13), and the detail description of the training procedures is presented in the subsequent section.

C. ANFIS-POD CONTROLLER TRAINING
To train the ANFIS based POD controller, the training data sets were collected from the non-adaptive POD controller implemented at the ESS controller. The test system was simulated for different values of the POD controller gains (K_D), and 5000 training and testing data points were obtained to design the ANFIS controller. Mode 1 IM loading configuration is connected to the AC sub-grid of the hybrid microgrid as the dynamic loads. Gaussian MF is used here, and MF parameters are tuned by 70% of the total collected data
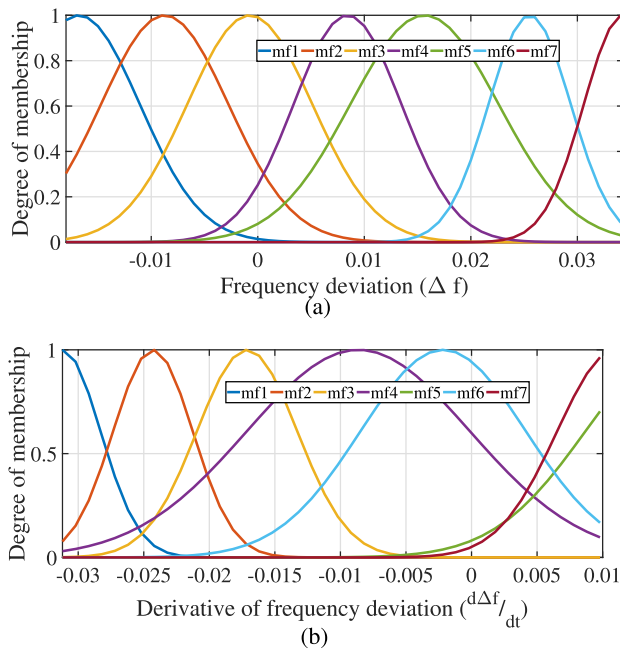
FIGURE 8. MF after training; (a) Frequency deviation (b) Derivative of frequency deviation.

(i.e., training data set). The initial FIS structure created by the grid partitioning technique, and back propagation algorithm is used for training. Before starting the training, the number of training epochs is selected as 100 and the model over-fitting was closely observed. The rest of the data set (30% of the collected data), including the testing data set (15% data), checking data set (15% data) is used to validate the trained FIS structure [31]. The MF of the frequency deviation after training is shown in Fig. 8 (a), while Fig. 8 (b) shows the MF of derivative of frequency deviation after training. After training, the Δf and the $\frac{d\Delta f}{dt}$ MFs are varied between -0.018 to 0.0343 and -0.0312 to 0.0099 respectively.

The proposed ANFIS based POD controller is trained with mode 1 IM loading configuration (given in Table 1) and tested with untrained mode 2 & 3 IMs loading configuration under disturbances to demonstrate the robustness of the proposed approach. The detailed simulation results for the training and testing modes are presented in Section V.

V. SIMULATION RESULTS

Non-linear dynamic simulations have been performed to evaluate the effectiveness of the proposed ANFIS based adaptive POD controller of the ESS considering known & unknown set of IM loading configurations and disturbances in the hybrid AC/DC microgrid. The following scenarios are considered for dynamic simulation studies and analysis;

- Training mode (26.72% load disturbances at the AC sub-grid)
- Training mode (40.03% load disturbances at the DC sub-grid)

- Test mode-1 (26.72% load disturbances at the AC sub-grid)
- Test mode-2 (26.72% load disturbances at the AC sub-grid)
- Test mode-1 (40.03% load disturbances at the DC sub-grid)
- Test mode-2 (40.03% load disturbances at the DC sub-grid)
- Test mode-1 (outage of a solar-PV at the AC sub-grid)

A. TRAINING MODE (26.72% LOAD DISTURBANCES AT THE AC SUB-GRID)

Aforementioned, three types of IM configurations (see Table 1) are considered in this study and the ANFIS based adaptive POD controller was trained for mode-1 IM loading configuration (known as the training mode). The total generation capacity of the AC sub-grid is 1 MW, and it is operated at 82.3% loading condition (300 kW CPL, 150 kW constant impedance load, and 373 kW IM), while the DC sub-grid installed capacity is 650 kW and it is operated at 46.09% loading (225 kW as a constant impedance load and a 100 hp IM). The disturbances are created by adding a 300 kW load at $t = 2.0$ s in the AC sub-grid, and subsequently, it is removed at $t = 3.0$ s, and the performance of the proposed ANFIS based adaptive POD controller is recorded. The IM rotor speed and the AC sub-grid point of common coupling (PCC) voltage are illustrated in Fig. 9 (a) and (b) respectively, whereas Fig. 9 (c) and (d) depict the AC sub-grid system frequency and the ESS power output, respectively. The voltage & frequency oscillations in the AC sub-grid and the DC voltage oscillations in the DC sub-grid are caused by the load disturbances. The voltage & frequency oscillations in the AC sub-grid will cause rotor speed oscillations due to following reasons, 1) IM power consumption (both active and reactive power) is influenced by the stator voltage & rotor speed, 2) IM rotor speed oscillations are caused by frequency variations, and 3) the change of rotor speed will affect power consumption. Furthermore, the above issues are even more severe for a system with high penetration of dynamic loads with a combination of small, medium, and large IMs [15]. As highlighted in Section III the presence of multiple operating IMs introduces more non-linearity into the systems dynamics.

When an additional 300 kW load is connected to the AC sub-grid, the ESS supplies the required load power to the system based on the deviation of system voltage & frequency from the reference set point. It can be seen from the ESS output that with the same gain for both controllers, it injects more active power and ensures better response. More active power injection from the ESS to the AC sub-grid ensures better voltage profile during load disturbances which can be noticed from Fig. 9 (b). With the increase of IM loading level, more damping torque is required to damp out speed oscillations. The significant difference of the proposed controller with non-adaptive POD controller is that the proposed controller will change the gain based on the frequency deviation, while the non-adaptive controller has the same gain.
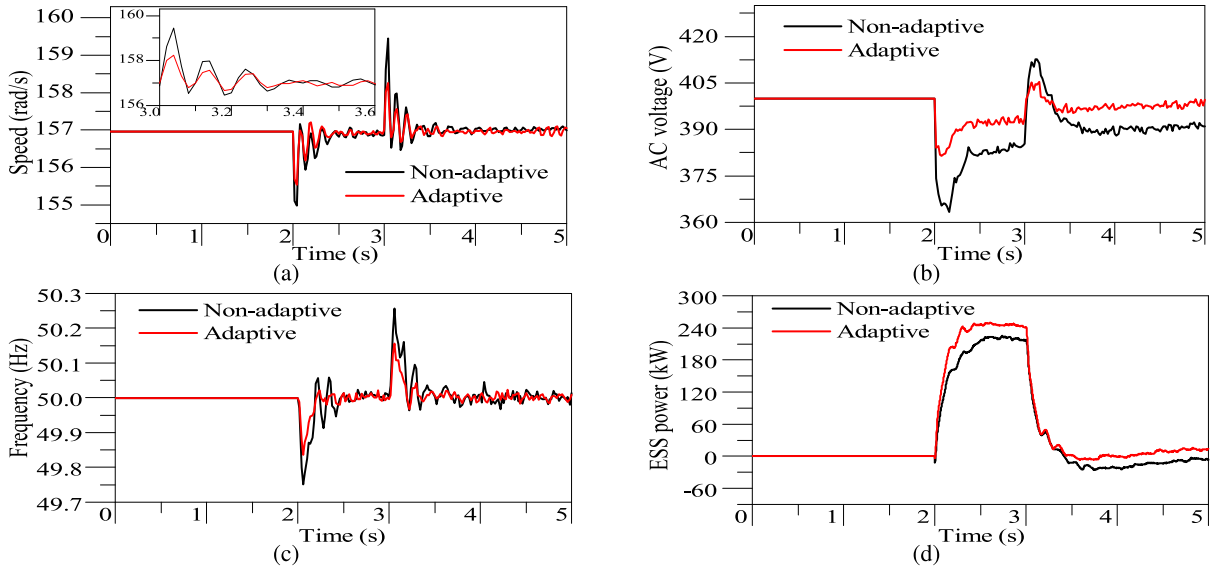
FIGURE 9. Hybrid AC/DC microgrid with training mode IM load under 26.72% load disturbances at the AC sub-grid, (a) IM rotor speed, (b) AC sub-grid PCC voltage, (c) AC sub-grid frequency, (d) ESS power injection to the AC sub-grid.
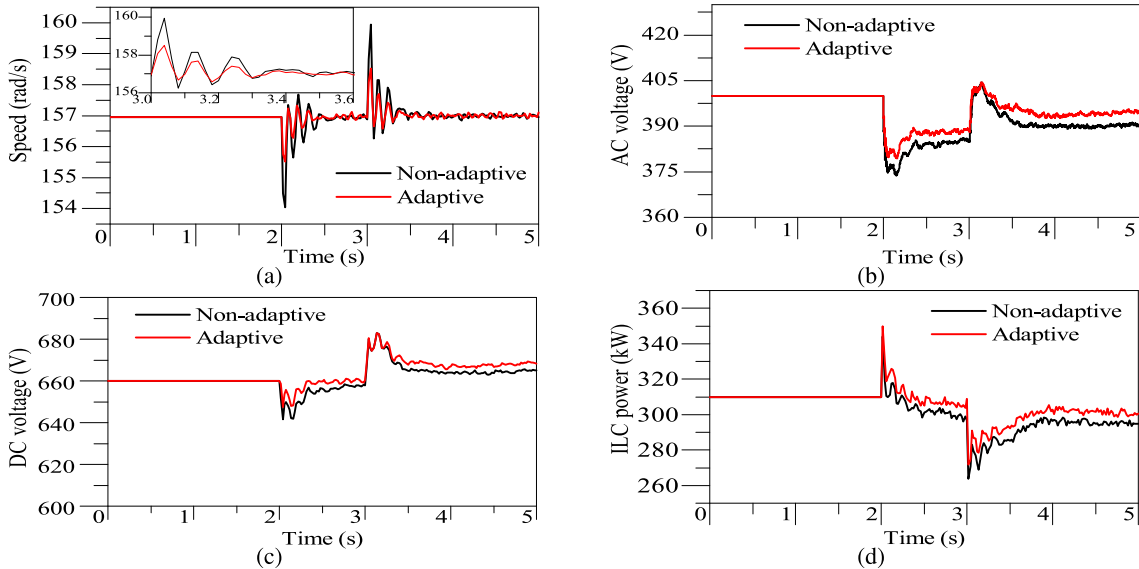

FIGURE 10. Hybrid AC/DC microgrid with mode 2 IM loading configuration under 26.72% load disturbances at the AC sub-grid (Test mode-1), (a) IM rotor speed, (b) AC sub-grid PCC voltage, (c) DC sub-grid PCC voltage, (d) The injected power to the AC sub-grid through ILC.

The rotor speed oscillation attenuation factor between the first and the forth peaks is utilized to identify the improvement of the damping performance of the proposed ANFIS based adaptive POD controller and the non-adaptive POD controller. The proposed controller has attenuated the speed oscillations by 88.71%, while it was 80.40% with a non-adaptive POD controller. Therefore, the proposed ANFIS based adaptive POD controller provides better damping attenuation factor compared to the non-adaptive POD controller. Moreover, the maximum frequency deviation during the 300 kW step load addition into the AC sub-grid is 49.84 Hz and 49.75 Hz for the ANFIS-POD controller and non-adaptive POD controller respectively. Furthermore, the proposed controller improved AC sub-grid voltage deviation

during the 300 kW step load addition into the AC sub-grid by 15 V compared to the non-adaptive POD controller. The performance comparison of the proposed controller in terms of rotor speed attenuation, maximum voltage, and frequency deviation during load disturbance is summarized in Table 2.

B. TRAINING MODE (40.03% LOAD DISTURBANCES AT THE DC SUB-GRID)

In this scenario, the AC sub-grid is connected with the same IM loading configuration used for the ANFIS-POD controller training. To further determine the effectiveness of the proposed ANFIS-POD controller, a 200 kW constant impedance load is connected to the DC sub-grid at $t = 2.0$ s, and subsequently removed at $t = 3.0$ s. When the additional 200 kW
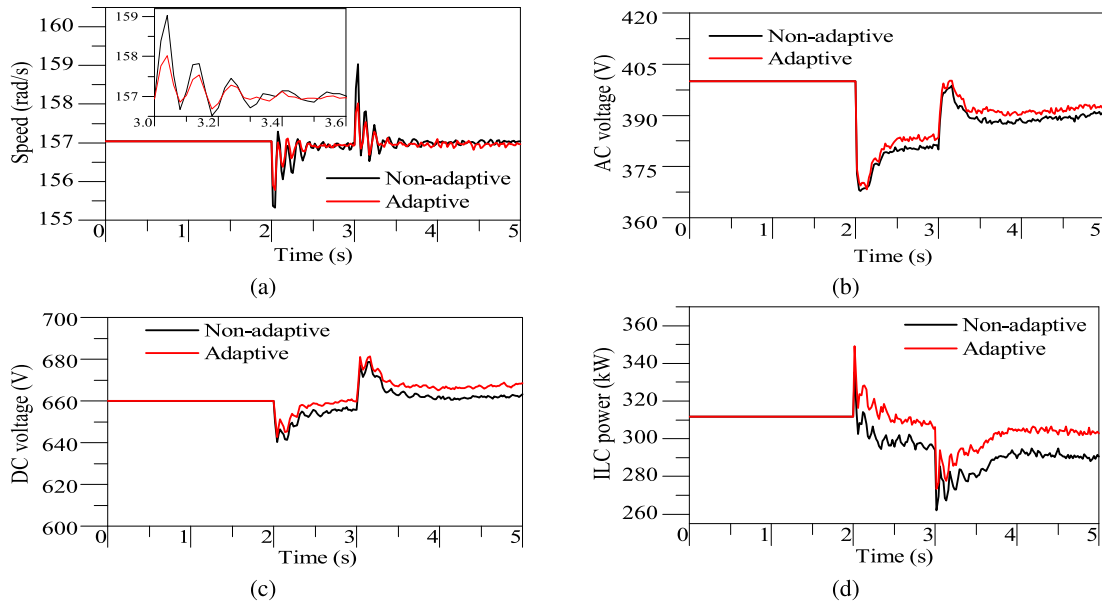
FIGURE 11. Hybrid AC/DC microgrid with mode 3 IM load under 26.72% load disturbances at the AC sub-grid (Test mode-2), (a) IM rotor speed, (b) AC sub-grid PCC voltage, (c) DC sub-grid PCC voltage, (d) The injected power to the AC sub-grid through ILC.

TABLE 2. Performance comparison.

	NA-POD controller	ANFIS-POD controller
Attenuation of speed oscillation	80.84%	88.71%
Maximum frequency deviation	49.75 Hz	49.84 Hz
Maximum voltage deviation	364 V	379 V

constant impedance load is connected to the DC sub-grid, this additional load is supplied by the DC sub-grid. Hence it reduces the power injection to the AC sub-grid from the DC sub-grid via the ILC. The power deficiency in the AC sub-grid is fulfilled by the ESS connected into the PCC of the AC sub-grid. As a consequence of this load disturbance; the AC and the DC voltages oscillate, and have resulted in IM rotor speed oscillations. Furthermore, additional dynamics have been introduced by adding a 100-hp IM via the DC to AC converter in the DC sub-grid as a CPL load. As highlighted in the literature, the CPL load causes poor damping and reduces the stability margin of the microgrid. Due to the negative resistance effect of the CPL load, it reduces the effective damping of the microgrid, hence instability occurs. The proposed ANFIS based POD controller has significantly damped oscillations and improved system stability margin.

C. TEST MODE-1 (26.72% LOAD DISTURBANCES AT THE AC SUB-GRID)

In this scenario, the effectiveness of the proposed ANFIS based POD controller is evaluated by adding a different (untrained) set of IM loading configuration (mode-2) known as test mode 1. As mentioned earlier, the ANFIS based POD controller was trained for mode 1 IM loading configuration

and its robustness was tested by applying a different set of IMs. With the different number of parallel operating IMs and their distinct power ratings have changed the entire dynamics of the hybrid AC/DC microgrid by introducing more non-linearity. It is important to note that IM configuration is different, but loading level is same as before and similar load disturbance as the previous scenario was applied. Fig. 10 (a) & (b) have been used to illustrate the IM rotor speed and the AC sub-grid PCC voltage respectively. Furthermore, Fig. 10 (c) & (d) demonstrate the DC sub-grid voltage and the ILC power injection to the AC sub-grid respectively.

An adaptive ANFIS based POD controller was trained for a set of IM loading, and when a different set of IM is connected to the system, it provides a better response compared to the non-adaptive POD controller. The inner current controller and outer voltage & frequency controller determine power deficiency in the AC sub-grid and required amount of power transfer to the AC sub-grid of the hybrid AC/DC microgrid. In addition, the proposed POD controller adds a supplementary control signal to the outer voltage control loop to damp out the rotor speed oscillations. The rotor speed oscillations are attenuated by 9.5% compared with a non-adaptive controller. Also, the proposed controller ensures small voltage dip and quick recovery of the AC & the DC sub-grid voltage following the load disturbance. Moreover, the sudden load addition have caused a power transfer disturbance at the ILC, which has been reduced by the proposed ANFIS based POD controller.

D. TEST MODE-2 (26.72% LOAD DISTURBANCES AT THE AC SUB-GRID)

The robustness of the proposed ANFIS-POD controller with another set of IM loading configuration (mode 3) known
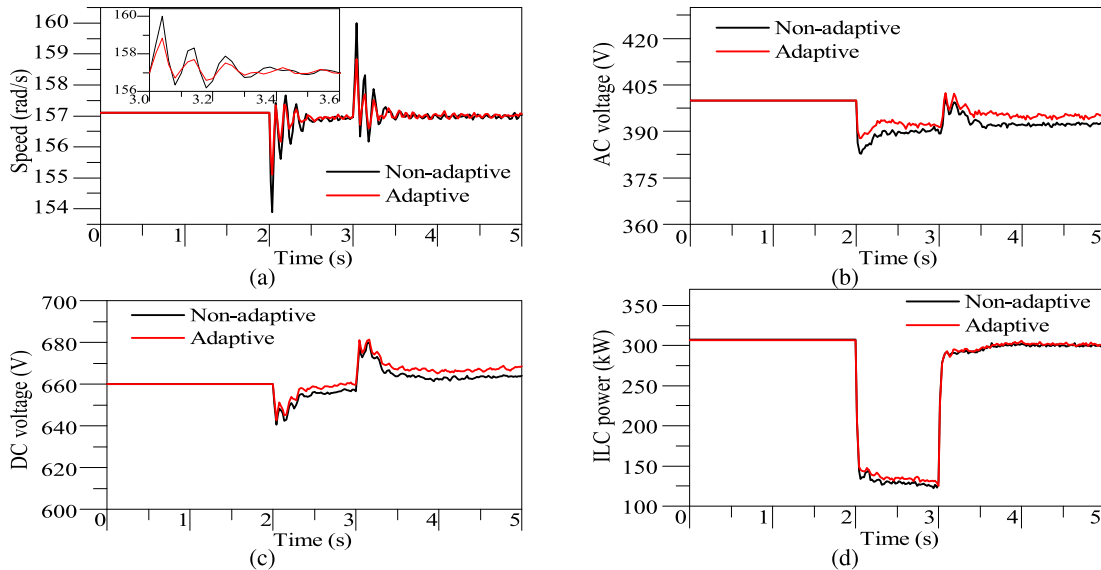
FIGURE 12. Hybrid AC/DC microgrid with mode 2 IM load under 40.03% load disturbances at the DC sub-grid (Test mode-1), (a) IM rotor speed, (b) AC sub-grid PCC voltage, (c) DC sub-grid PCC voltage, (d) The injected power to the AC sub-grid through ILC.

as test mode 2 is provided in this sub-section. Same as the previous scenario, previously trained ANFIS-POD controller with different untrained IM configurations are connected to the AC sub-grid, while IM loading level will remain the same. An additional 300 kW load is connected at $t = 2.0$ s and subsequently, removed at $t = 3$ s. The effect of the load disturbance on IM rotor speed and AC sub-grid voltage are illustrated in Fig. 11 (a) & (b) respectively. The effect of load disturbance on DC sub-grid voltage and ILC power injection from the DC sub-grid to the AC sub-grid through ILC are also illustrated in Fig. 11 (c) & (d) respectively.

The voltage and frequency oscillations are caused by the load disturbance which has given rise to AC sub-grid voltage oscillations, DC sub-grid voltage oscillations, and IM rotor speed oscillations. Fig. 11 (a) shows that for an un-trained set of IMs connected to the AC sub-grid, the proposed controller has damp out IM rotor speed oscillations by 10% compared to the non-adaptive controller. It is noteworthy that the voltage profile of both the AC & the DC sub-grid is better compared to the non-adaptive controller.

E. TEST MODE-1 (40.03% LOAD DISTURBANCES AT THE DC SUB-GRID)

In this scenario, an un-trained set of IM loading configuration (mode 2) known as the test mode 1 is connected to the AC sub-grid. The effectiveness of the proposed ANFIS-POD control scheme is evaluated through a connection (at $t = 2.0$ s) and disconnection (at $t = 3.0$ s) of a 200 kW constant impedance load at the DC sub-grid of the hybrid AC/DC microgrid. Fig. 12 (a) & (b) show the response of the IM rotor and the PCC voltage of the AC sub-grid for this case. Fig. 12 (c) & (d) depict the comparison of the DC sub-grid voltage & ILC power injection between the non-adaptive and

adaptive controller. An energy imbalance at the DC sub-grid is transferred through the ILC into the AC sub-grid and subsequently leads to DC bus voltage oscillations, AC sub-grid voltage oscillations, and rotor speed oscillations. Moreover, different number of parallel operating IMs with various power ratings have changed the dynamics of the entire hybrid AC/DC microgrid by introducing more non-linearity. Fig. 12 (a) shows that the ESS with adaptive POD controller has resulted in lower IM rotor speed oscillations and small AC sub-grid voltage dip during load perturbations by injecting required amount of active power.

F. TEST MODE-2 (40.03% LOAD DISTURBANCES AT THE DC SUB-GRID)

In this sub-section, the robustness of the proposed ANFIS-POD controller is analysed with large load disturbance using an un-trained set of IM loading configuration (test mode 2). As similar to the previous scenario, the number of parallel operating IMs have changed, but the entire IM loading level remains unchanged. The performance of the IM rotor and AC sub-grid PCC voltage under a step change of the load are investigated, as shown in Fig. 13 (a) and (b), where the load is connected to the DC sub-grid at $t = 2.0$ s, and subsequently removed at $t = 3.0$ s. Fig. 13 (c) and (d) show the DC sub-grid voltage and the ILC power injection to the AC sub-grid with the non-adaptive and adaptive POD controller.

As can be seen from Fig. 13 (a), the load disturbances yield rotor speed oscillations of small amplitude with the proposed controller. Hence the supplementary ANFIS-POD controller of the ESS is capable of damping the IM rotor speed oscillations yielding better AC and DC sub-grid voltage responses. The PSD analysis of the system frequency
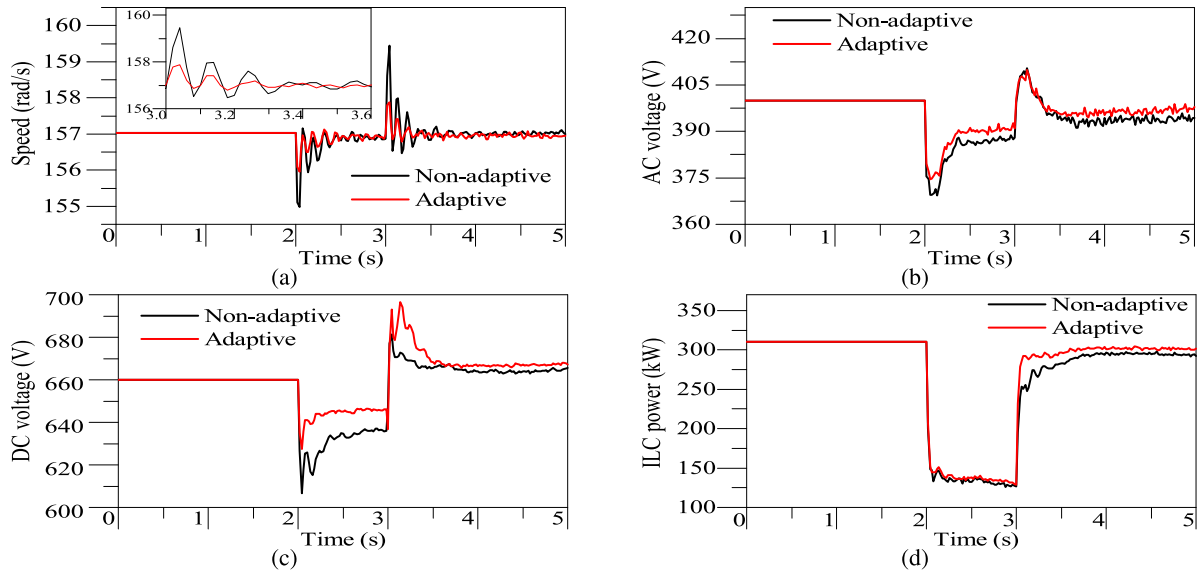
FIGURE 13. Hybrid AC/DC microgrid with mode 3 IM load under 40.03% load disturbances at the DC sub-grid (Test mode-2), (a) IM rotor speed, (b) AC sub-grid PCC voltage, (c) DC sub-grid PCC voltage, (d) The injected power to the AC sub-grid via the ILC.
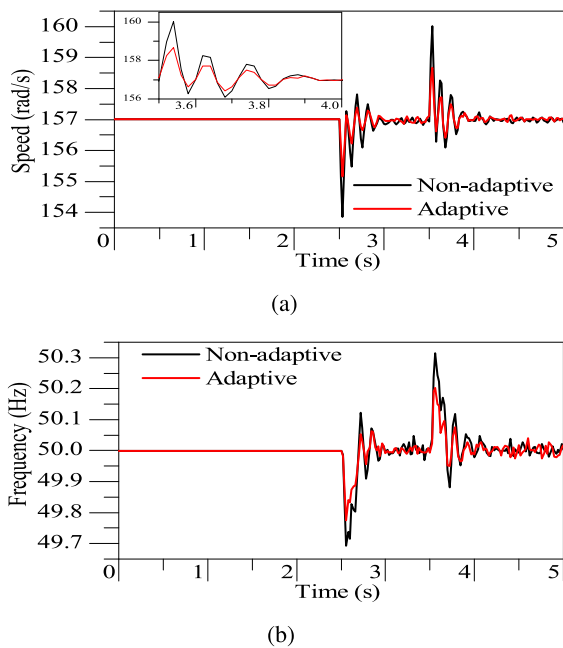

FIGURE 14. Hybrid AC/DC microgrid with mode-2 IM load under outage of a solar-PV at the AC sub-grid (Test mode-1), (a) IM rotor speed, (b) AC sub-grid frequency.

with different IM loading configuration (i.e., training mode, un-trained mode 1 & 2) indicates that for each IM configuration, the system dynamics is different as the IM load dominates the hybrid AC/DC microgrid system dynamics. The proposed ANFIS-POD controller intelligently recognises the non-linear dynamics of the hybrid microgrid system due to the changing nature of IM loads (i.e., dynamic loads) and adjust its gain which has resulted in better attenuation of rotor speed oscillations and improved voltage profile.

G. TEST MODE-1 (OUTAGE OF A 250 *kW* SOLAR-PV AT THE AC SUB-GRID)

In this scenario, an un-trained set of IM loading configuration (mode 2) known as the test mode 1 is connected to the AC sub-grid. The effectiveness of the proposed ANFIS-POD control scheme is evaluated through an outage (at $t = 2.5$ s) and re-connection (at $t = 3.5$ s) of a 250 kW solar-PV at the AC sub-grid of the hybrid AC/DC microgrid. Fig. 14 (a) & (b) show the response of the IM rotor speed and the frequency of the AC sub-grid for this case. When the 250 kW solar-PV is disconnected from the AC sub-grid at $t = 2.5$ s, it has caused a generation and load-demand imbalance at the microgrid (from $t = 2.5$ s to 3.5 s). This imbalance was sensed by the ESS and it supplied the additional load-demand. The supplementary ANFIS-POD controller of the ESS has effectively dampen the rotor speed oscillations and frequency response. Therefore, the supplementary ANFIS-POD controller is effectively damping oscillations even for untrained scenarios.

VI. CONCLUSION

This paper has investigated the LFO issue in hybrid AC/DC microgrids with various combinations of small, medium, and large IMs and proposed an ANFIS based POD controller to mitigate the oscillations. A PSD analysis was performed on the system frequency by considering two scenarios: 1) a single large IM & multiple small IMs, 2) a combination of parallel operating small, medium, and large IMs. It was revealed that the multiple parallel operating IMs adds more non-linearity into the system dynamics. Moreover, the increase of dynamic loads (i.e., IMs) leads to more rotor speed oscillations and frequency deviations in the hybrid AC/DC microgrid and hence more damping torque is required. However, the gain of conventional POD controllers is fixed

and can't adapt to the changes in the microgrid load composition. These key findings have been used to design a supplementary ANFIS-POD controller to provide additional damping torque proportional to the frequency deviation and damp the LFOs. The following conclusions can be drawn from this study;

- The IM rotor speed oscillations increase with the increase of the IM loading level; hence more damping torque is required to damp out the speed oscillations.
- Any disturbance in either side of the hybrid AC/DC microgrid would cause energy imbalance that leads to IM rotor speed oscillations which is significantly damped by the proposed ANFIS-POD controller.
- Any disturbance in either side of the hybrid AC/DC microgrid would cause energy imbalance, which leads to voltage & frequency oscillations at the AC and the DC sub-grids, which are significantly improved by the proposed ANFIS-POD controller.
- The ANFIS based POD controller autonomously adjusts its gain based on the frequency deviation and IM loading level. The robustness of the proposed controller is verified by applying various disturbances and unknown combinations of parallel operating IMs of distinct power ratings.

APPENDIX

Hybrid AC/DC Microgrid DER parameters are taken from [16]

POD controller parameters:

$K_D = 150$, $T_1 = 0.1$ s, $T_w = 10$ s.

5-hp IM parameters:

$R_r = 0.01909$ pu, $R_s = 0.01965$ pu, $H = 0.09526$ pu, $L_r = 0.0397$ pu, $L_s = 0.0397$ pu, $P = 2$, and $L_m = 1.354$ pu.

10-hp IM parameters:

$R_r = 0.02067$ pu, $R_s = 0.02013$ pu, $H = 0.08389$ pu, $L_r = .02919$ pu, $L_s = 0.02919$ pu, $P = 2$, and $L_m = 1.89$pu.

15-hp IM parameters:

$R_r = 0.0094$ pu, $R_s = 0.014$ pu, $H = 0.15$ pu, $L_r = 0.012$ pu, $L_s = 0.012$ pu, $P = 2$, and $L_m = .98$ pu.

20-hp IM parameters:

$R_r = 0.0347$ pu, $R_s = 0.0346$ pu, $H = 0.0564$ pu, $L_r = 0.0448$ pu, $L_s = 0.0448$ pu, $P = 2$, and $L_m = 1.827$pu.

25-hp IM parameters:

$R_r = 0.04724$ pu, $R_s = 0.02194$ pu, $H = 0.527719$ pu, $L_r = 0.005305$ pu, $L_s = 0.0053$ pu, $P = 2$, and $L_m = 0.00517$ pu.

50-hp IM parameters:

$R_r = 0.04019$ pu, $R_s = 0.015336$ pu, $H = 0.791579$ pu, $L_r = 0.05323$ pu, $L_s = 0.05323$ pu, $P = 2$, and $L_m = 2.30568$ pu.

200-hp IM parameters:

$R_r = 0.009956\Omega$, $R_s = 0.014\Omega$, $J = 3.5$ $kg.m^2$, $L_r = 0.00019$ H, $L_s = 0.00019$ H, and, $L_m = 0.00945$ H.

cable parameters:

cable reactance $= 0.08$ Ω /km, cable resistance $= 0.2$ Ω /km.

REFERENCES

[1] M. A. Hossain, H. R. Pota, M. J. Hossain, and F. Blaabjerg, "Evolution of microgrids with converter-interfaced generations: Challenges and opportunities," *Int. J. Electr. Power Energy Syst.*, vol. 109, pp. 160–186, Jul. 2019.

[2] D. R. Prathapaneni and K. P. Detroja, "An integrated framework for optimal planning and operation schedule of microgrid under uncertainty," *Sustain. Energy, Grids Netw.*, vol. 19, Sep. 2019, Art. no. 100232.

[3] I. Worighi, A. Maach, A. Hafid, O. Hegazy, and J. Van Mierlo, "Integrating renewable energy in smart grid system: Architecture, virtualization and analysis," *Sustain. Energy, Grids Netw.*, vol. 18, Jun. 2019, Art. no. 100226.

[4] J. Rocabert, A. Luna, F. Blaabjerg, and P. Rodriguez, "Control of power converters in AC microgrids," *IEEE Trans. Power Electron.*, vol. 27, no. 11, pp. 4734–4749, Nov. 2012.

[5] A. V. Jayawardena, L. G. Meegahapola, S. Perera, and D. A. Robinson, "Dynamic characteristics of a hybrid microgrid with inverter and non-inverter interfaced renewable energy sources: A case study," in *Proc. IEEE Int. Conf. Power Syst. Technol. (POWERCON)*, Auckland, New Zealand, Oct. 2012, pp. 1–6.

[6] D. K. Dheer, N. Soni, and S. Doolla, "Improvement of small signal stability margin and transient response in inverter-dominated microgrids," *Sustain. Energy, Grids Netw.*, vol. 5, pp. 135–147, Mar. 2016.

[7] N. Pogaku, M. Prodanovic, and T. C. Green, "Modeling, analysis and testing of autonomous operation of an inverter-based microgrid," *IEEE Trans. Power Electron.*, vol. 22, no. 2, pp. 613–625, Mar. 2007.

[8] E. A. A. Coelho, P. C. Cortizo, and P. F. D. Garcia, "Small-signal stability for parallel-connected inverters in stand-alone AC supply systems," *IEEE Trans. Ind. Appl.*, vol. 38, no. 2, pp. 533–542, Mar. 2002.

[9] M. Ahmed, A. Vahidnia, L. Meegahapola, and M. Datta, "Small signal stability analysis of a hybrid AC/DC microgrid with static and dynamic loads," in *Proc. Australas. Universities Power Eng. Conf. (AUPEC)*, Melbourne, VIC, Australia, Nov. 2017, pp. 1–6.

[10] M. Ahmed, L. Meegahapola, A. Vahidnia, and M. Datta, "Analyzing the effect of X/R ratio on dynamic performance of microgrids," in *Proc. IEEE PES Innov. Smart Grid Technol. Eur. (ISGT-Europe)*, Bucharest, Romania, Sep. 2019, pp. 1–5.

[11] M. Ahmed, L. Meegahapola, A. Vahidnia, and M. Dutta, "Influence of feeder characteristics on hybrid ac/dc microgrids stability," in *Proc. 9th Int. Conf. Power Energy Syst. (ICPES)*, Perth, WA, Australia, Dec. 2019.

[12] *Annual Energy Outlook 2011: With Projections to 2035*. UEI Admin., Government Printing Office, Washington, DC, USA, 2011.

[13] B. M. Nomikos and C. D. Vournas, "Investigation of induction machine contribution to power system oscillations," *IEEE Trans. Power Syst.*, vol. 20, no. 2, pp. 916–925, May 2005.

[14] J. V. Milanovic and I. A. Hiskens, "Effects of load dynamics on power system damping," *IEEE Trans. Power Syst.*, vol. 10, no. 2, pp. 1022–1028, May 1995.

[15] M. Ahmed, A. Vahidnia, L. Meegahapola, and M. Datta, "Impact of multiple motor loads on dynamic performance and stability of microgrids," in *Proc. IEEE Int. Conf. Ind. Technol. (ICIT)*, Melbourne, VIC, Australia, Feb. 2019, pp. 1704–1709.

[16] M. Ahmed, L. Meegahapola, A. Vahidnia, and M. Datta, "Analysis and mitigation of low-frequency oscillations in hybrid AC/DC microgrids with dynamic loads," *IET Gener., Transmiss. Distrib.*, vol. 13, no. 9, pp. 1477–1488, May 2019.

[17] J. M. Espi, J. Castello, R. García-Gil, G. Garcera, and E. Figueres, "An adaptive robust predictive current control for three-phase grid-connected inverters," *IEEE Trans. Ind. Electron.*, vol. 58, no. 8, pp. 3537–3546, Aug. 2011.

[18] H. Li, K. L. Shi, and P. G. McLaren, "Neural-network-based sensorless maximum wind energy capture with compensated power coefficient," *IEEE Trans. Ind. Appl.*, vol. 41, no. 6, pp. 1548–1556, Nov. 2005.

[19] J.-S. R. Jang, "ANFIS: Adaptive-network-based fuzzy inference system," *IEEE Trans. Syst., Man, Cybern.*, vol. 23, no. 3, pp. 665–685, Jun. 1993.

[20] S. R. Khuntia and S. Panda, "ANFIS approach for SSSC controller design for the improvement of transient stability performance," *Math. Comput. Model.*, vol. 57, nos. 1–2, pp. 289–300, Jan. 2013.

[21] L. Cai and I. Erlich, "Coordination between transient and damping controller for series facts devices using ANFIS technology," *IFAC Proc. Volumes*, vol. 36, no. 20, pp. 293–298, Sep. 2003.

[22] H. Bevrani and S. Shokoohi, "An intelligent droop control for simultaneous voltage and frequency regulation in islanded microgrids," *IEEE Trans. Smart Grid*, vol. 4, no. 3, pp. 1505–1513, Sep. 2013.

[23] L. Meegahapola and D. Robinson, "Smart power systems and renewable energy system integration," in *Dynamic Modelling, Simulation and Control of a Commercial Building Microgrid*. Cham, Switzerland: Springer, 2016.

[24] W. W. Price, K. A. Wirgau, A. Murdoch, J. V. Mitsche, E. Vaahedi, and M. El-Kady, "Load modeling for power flow and transient stability computer studies," *IEEE Trans. Power Syst.*, vol. PWRS-3, no. 1, pp. 180–187, Feb. 1988.

[25] P. Kundur, N. J. Balu, and M. G. Lauby, *Power System Stability and Control*, vol. 7. New York, NY, USA: McGraw-Hill, 1994.

[26] W. Peres, "Multi-band power oscillation damping controller for power system supported by static VAR compensator," *Electr. Eng.*, vol. 101, no. 3, pp. 943–967, Sep. 2019.

[27] A. Khodabakhshian, R. Hemmati, and M. Moazzami, "Multi-band power system stabilizer design by using CPCE algorithm for multi-machine power system," *Electr. Power Syst. Res.*, vol. 101, pp. 36–48, Aug. 2013.

[28] D. Rimorov, A. Heniche, I. Kamwa, G. Stefopoulos, S. Babaei, and B. Fardanesh, "Inter-area oscillation damping and primary frequency control of the new york state power grid with multi-functional multi-band power system stabilizers," in *Proc. IEEE Power Energy Soc. Gen. Meeting (PESGM)*, Boston, MA, USA, Jul. 2016, pp. 1–5.

[29] J. S. R. Jang, C. T. Sun, and E. Mizutani, "Neuro-fuzzy and soft computing—A computational approach to learning and machine intelligence [book review]," *IEEE Trans. Autom. Control*, vol. 42, no. 10, pp. 1482–1484, Oct. 1997.

[30] A. K. Jain, J. Mao, and K. M. Mohiuddin, "Artificial neural networks: A tutorial," *Computer*, vol. 29, no. 3, pp. 31–44, Mar. 1996.

[31] A. Taher, "Adaptive neuro-fuzzy systems," in *Fuzzy Systems*. Rijeka, Croatia: InTech, Feb. 2010.

ARASH VAHIDNIA (Senior Member, IEEE) received the Ph.D. degree in power engineering from the Queensland University of Technology (QUT). He was a Research Fellow with the Power Engineering Group, QUT, before joining RMIT. He also has several years of industry experience working with power consultancy and utility firms. He is currently a Lecturer with the School of Engineering, RMIT University. His research interest includes power system stability, reliability, microgrids, renewable energies, and system planning and control.

MANOJ DATTA (Senior Member, IEEE) received the Ph.D. degree in interdisciplinary intelligent systems engineering from Japan, in 2011. From 2011 to 2012, he was a JSPS Postdoctoral Research Fellow with the Faculty of Engineering, University of the Ryukyus, Japan. From 2012 to 2013, he was an Assistant Professor with the Department of Human and Information Systems, Gifu University, Japan. Since late 2013, he has been with the School of Electrical and Computer Engineering, RMIT University, Melbourne, VIC, Australia. His research interests include motor drives, distributed generation forecasting, microgrid modeling, grid integration of DGs, and intelligent ancillary services in the smart grid. He is a member of the Institute of Electrical Engineers, Japan. He was a recipient of the University of the Ryukyus President's Honorary Award for an outstanding Ph.D. thesis.

LASANTHA MEEGAHAPOLA (Senior Member, IEEE) received the B.Sc. Eng. degree (Hons.) in electrical engineering from the University of Moratuwa, Sri Lanka, in 2006, and the Ph.D. degree from the Queen's University of Belfast, U.K., in 2010. His Ph.D. degree was based on the investigation of power system stability issues with high-wind penetration, and research was conducted in collaboration with EirGrid (Republic of Ireland-TSO). He has more than ten years of research experience in power system dynamics and stability with renewable power generation. He has also conducted research studies on microgrid dynamics and stability, and coordinated reactive power dispatch during steady-state and dynamic/transient conditions for networks with high wind penetration. He was a Visiting Researcher with the Electricity Research Centre, University College Dublin, Ireland, from 2009 to 2010. From 2011 to 2014, he was employed as a Lecturer with the University of Wollongong (UOW), where he is currently continues as an Honorary Fellow. He is also employed as a Senior Lecturer with the Royal Melbourne Institute of Technology (RMIT) University. He has published more than 80 journal and conference papers. He is a Member of the IEEE Power and Energy Society (PES).

MOUDUD AHMED (Student Member, IEEE) received the B.Sc. degree (Hons.) in electrical engineering from the Chittagonj University of Engineering and Technology, Bangladesh, in 2012, and the M.Sc. degree in electrical and electronic engineering from the Khulna University of Engineering and Technology, Bangladesh, in 2016. He is currently pursuing the Ph.D. degree with the Royal Melbourne Institute of Technology (RMIT) University, Melbourne, VIC, Australia. His current research interests include hybrid AC/DC microgrid stability and power system control. He is a member of the IEEE Power and Energy Society (PES).

● ● ●